NASA / CR—1999-209311

Multistage Simulations of the GE90 Turbine

Mark G. Turner
GE Aircraft Engines, Cincinnati, Ohio

Paul H. Vitt
ASE Technologies, Cincinnati, Ohio

David A. Topp, Sohrab Saeidi, Scott D. Hunter, Lyle D. Dailey
GE Aircraft Engines, Cincinnati, Ohio

Timothy A. Beach
Dynacs Engineering Company, Inc., Brook Park, Ohio

September 1999

The NASA STI Program Office . . . in Profile

Since its founding, NASA has been dedicated to the advancement of aeronautics and space science. The NASA Scientific and Technical Information (STI) Program Office plays a key part in helping NASA maintain this important role.

The NASA STI Program Office is operated by Langley Research Center, the Lead Center for NASA's scientific and technical information. The NASA STI Program Office provides access to the NASA STI Database, the largest collection of aeronautical and space science STI in the world. The Program Office is also NASA's institutional mechanism for disseminating the results of its research and development activities. These results are published by NASA in the NASA STI Report Series, which includes the following report types:

- TECHNICAL PUBLICATION. Reports of completed research or a major significant phase of research that present the results of NASA programs and include extensive data or theoretical analysis. Includes compilations of significant scientific and technical data and information deemed to be of continuing reference value. NASA's counterpart of peer-reviewed formal professional papers but has less stringent limitations on manuscript length and extent of graphic presentations.

- TECHNICAL MEMORANDUM. Scientific and technical findings that are preliminary or of specialized interest, e.g., quick release reports, working papers, and bibliographies that contain minimal annotation. Does not contain extensive analysis.

- CONTRACTOR REPORT. Scientific and technical findings by NASA-sponsored contractors and grantees.

- CONFERENCE PUBLICATION. Collected papers from scientific and technical conferences, symposia, seminars, or other meetings sponsored or cosponsored by NASA.

- SPECIAL PUBLICATION. Scientific, technical, or historical information from NASA programs, projects, and missions, often concerned with subjects having substantial public interest.

- TECHNICAL TRANSLATION. English-language translations of foreign scientific and technical material pertinent to NASA's mission.

Specialized services that complement the STI Program Office's diverse offerings include creating custom thesauri, building customized data bases, organizing and publishing research results . . . even providing videos.

For more information about the NASA STI Program Office, see the following:

- Access the NASA STI Program Home Page at ***http://www.sti.nasa.gov***

- E-mail your question via the Internet to help@sti.nasa.gov

- Fax your question to the NASA Access Help Desk at (301) 621-0134

- Telephone the NASA Access Help Desk at (301) 621-0390

- Write to:
  NASA Access Help Desk
  NASA Center for AeroSpace Information
  7121 Standard Drive
  Hanover, MD 21076

NASA / CR—1999-209311

Multistage Simulations of the GE90 Turbine

Mark G. Turner
GE Aircraft Engines, Cincinnati, Ohio

Paul H. Vitt
ASE Technologies, Cincinnati, Ohio

David A. Topp, Sohrab Saeidi, Scott D. Hunter, Lyle D. Dailey
GE Aircraft Engines, Cincinnati, Ohio

Timothy A. Beach
Dynacs Engineering Company, Inc., Brook Park, Ohio

Prepared for the
1999 International Gas Turbine and Aeroengine Congress
cosponsored by the American Society of Mechanical Engineers and
the International Gas Turbine Institute
Indianapolis, Indiana, June 7–10, 1999

Prepared under Contract NAS3–26617

National Aeronautics and
Space Administration

Glenn Research Center

September 1999

Acknowledgments

The authors wish to acknowledge support of this work from the NASA AST program (contract number NAS3–27720, AIO5) and from the NASA Glenn Research Center NPSS (Numerical Propulsion System Simulation) program (contract NAS3–26617 LET#65). Support by NASA HPCCP (High Performance Computing and Communications Program) and the CAS (Computational Aerosciences) Project is also appreciated. Personal thanks go to John Adamczyk, Joseph P. Veres and John Lytle of the NASA Glenn Research Center. Thanks also to Larry Timko and Rob Beacock of GE for guidance on the GE90 turbines.

Available from

NASA Center for Aerospace Information
7121 Standard Drive
Hanover, MD 21076
Price Code: A03

National Technical Information Service
5285 Port Royal Road
Springfield, VA 22100
Price Code: A03

MULTISTAGE SIMULATIONS OF THE GE90 TURBINE

Mark G. Turner
GE Aircraft Engines
Cincinnati, OH

Paul H. Vitt
ASE Technologies
Cincinnati, OH

David A. Topp, Sohrab Saeidi, Scott D. Hunter, Lyle D. Dailey
GE Aircraft Engines
Cincinnati, OH

Timothy A. Beach
Dynacs Engineering Company, Inc.
Brook Park, OH

ABSTRACT

The average passage approach has been used to analyze three multistage configurations of the GE90 turbine. These are a high pressure turbine rig, a low pressure turbine rig and a full turbine configuration comprising 18 blade rows of the GE90 engine at takeoff conditions. Cooling flows in the high pressure turbine have been simulated using source terms. This is the first time a dual-spool cooled turbine has been analyzed in 3D using a multistage approach. There is good agreement between the simulations and experimental results. Multistage and component interaction effects are also presented. The parallel efficiency of the code is excellent at 87.3% using 121 processors on an SGI Origin for the 18 blade row configuration. The accuracy and efficiency of the calculation now allow it to be effectively used in a design environment so that multistage effects can be accounted for in turbine design.

INTRODUCTION

The high pressure turbine (HPT) of a modern turbofan engine must operate in an extreme environment of high temperature, high stress, and high speed. As such, it must be film cooled and designed for long life and high efficiency. The heat transfer design requires a detailed knowledge of the gas side temperatures. The low pressure turbine (LPT) is designed for very high efficiency and must be able to operate effectively behind the HPT. The requirements for both the HPT and LPT necessitate a detailed aerodynamic solution capability which accounts for the film cooling, multistage effects and variable gas properties.

The Average Passage Approach developed by Adamczyk (1986) has been generalized for improved grids by Kirtley, Turner and Saeidi (1999) and applied to the complete turbine for the GE90 turbofan engine. In preparation for doing the full turbine, the HPT and LPT rig configurations were first validated. These rigs were designed and tested as part of the GE90 development program. A three quarter scale rig of the 2 stage GE90 HPT was designed and built by GE and tested at the NASA Glenn Research Center. A half scale rig of the 6 stage GE90 LPT was designed and built by GE and Fiat and tested at GE. These rig tests produced detailed measurements of hub and casing static pressures and inlet and exit profiles of total pressure, total temperature and flow angles. The engine turbine simulation was set up based upon a cycle analysis of the GE90 engine at takeoff. The HPT rig simulation comprised 4 blade rows; the LPT rig was 14 blade rows including the mid frame strut and OGV, and the full turbine simulation comprised all 18 blade rows.

The present work was undertaken for three reasons:

1. To support a full engine simulation of the GE90 in order to demonstrate the capability of high fidelity 3D analysis for a complete turbofan application. This would allow an analysis of the primary flowpath when coupled with the full compression system and a model of the combustor. This represents the first time a dual-spool cooled turbine has been analyzed using a 3D multistage solver.
2. To determine the differences between a turbine running at warm air rig conditions and that running in an engine. For the HPT, this involves a severe inlet temperature profile at elevated temperatures. For the LPT, this involves the interaction with the upstream HPT which produces profiles of temperature, pressure and flow angles. The amount of cavity purge flows in an engine application were also much greater than in the LPT rig, which greatly modifies the hub aerodynamics in the LPT.
3. To validate the method for application in turbine design by simulating real turbine hardware.

This paper describes the features of the code, APNASA, including film cooling and the variable gas model used. It also presents the method of simulating leakage flows due to purge cavity flows, nozzle under shroud leakages and rotor over shroud leakages. Following this, the HPT rig, the LPT rig and the full engine configurations will be described. Results for these simulations will then be presented with particular emphasis on multistage effects and

differences between rig and engine simulations. Following the results is a description of the parallel capability of the solver when applied to the 18 blade row full turbine configuration.

METHODOLOGY

Researchers have used three methods for multistage analysis. These include the mixing plane approach as described by Dawes (1990), the average passage approach of Adamczyk (1986), and the fully unsteady approach similar to Chen, Celestina and Adamczyk (1994). A full unsteady analysis for a problem of this scale is still beyond the computing capability currently available. The mixing plane approach produces an entropy jump at the mixing plane as demonstrated by Fritsch and Giles (1993). Especially for HPT turbines with large circumferential variations, this can lead to large errors. Therefore, the average passage approach has been used to simulate the multistage environment of the turbine. This has been shown by Turner (1996) to work well for an LPT application. The ability of this approach to capture most of the multistage effects is presented by Adamczyk (1999).

Numerical Scheme

The foundation of the Navier-Stokes solver is an explicit 4 stage Runge-Kutta scheme with local time stepping and implicit residual smoothing to accelerate convergence. Second and fourth difference smoothing as applied by Jameson (1984) is employed for stability and shock capturing. A k-ε turbulence model is solved using an implicit upwind approach similar to that presented by Turner and Jennions (1992) and Shabbir et. al. (1997). Wall functions are employed to model the turbulent shear stress adjacent to the wall without the need to resolve the entire boundary layer.

The solver has been parallelized using MPI (Message Passing Interface) to share information across domain boundaries. Domain decomposition is accomplished "on the fly" by subdividing the grid in the axial direction into an arbitrary number of domains specified in the argument list. The number of parallel bugs has been reduced or totally eliminated by strict adherence to keep the parallel code equal to serial (within numerical precision). The overall solver has two levels of parallel capability as shown in Figure 1. The first level is to solve each blade row in a multistage component. The next level is to solve each blade row on several processors.

All blade rows are run for 50-100 Runge-Kutta iterations, at which time the body forces and deterministic stresses are calculated and written to a file. This is one outer iteration, or flip. At this time, the files are distributed to the other blade rows to update the multistage effects.

Average Passage Approach with Generalized Closure

A more general form of the average passage closure first developed by Adamczyk (see Adamczyk, Celestina and Mulac (1986)) has been developed by Kirtley, Turner and Saeidi (1999). It allows for non-pure H grids, as shown in Figure 2 for the GE90 HPT rotor 1. These grids have been generated using APG, a grid generator specially designed for the Average Passage Code with the generalized closure implementation. Compared with the pure H-grids required by the previous closure implementation, these grids allow much better leading and trailing edge orthogonality and resolution which improves accuracy and the convergence rate. The closure requires overlapping grids so that the deterministic stresses from one blade row are applied to other blade rows. This allows blade row interactions such as spanwise mixing of temperature, wake blockage and potential field blockage due to blunt leading edges to be modeled.

The desired near wall grid spacing can be characterized by the dimensionless quantity y^+ which should be approximately 30 when wall functions are used. Grid generation was carried out with this goal in mind, while also balancing the need for good leading and trailing edge resolution. The actual y^+ values on the pressure surface of Nozzle 1 were approximately 20. Tip gaps over the unshrouded HPT rotors have been modeled with 4 cells. Periodicity is applied across a void representing an extrusion of the blade to the casing. Overall grid resolution has been set based on a detailed grid study of the LPT nozzle 1 as an isolated blade row. Grids were chosen which produced accurate flowrate and loss calculations. This gridding approach was then applied for all blade rows. The resulting grids had 50 spanwise grid points. The number of blade-to-blade grid points varied with blade row solidity; 41 blade-to-blade grid points is a representative number. A minimum of 72 points from leading to trailing edge were used. The number of grid points in the axial direction varied depending on the chord and axial gaps of each individual airfoil.

As mentioned, the average passage approach uses overlapping grids. When validating the HP turbine, it was noticed that the extent of that overlap should only be half way through the downstream blade row. If the overlap extends further, the upstream blade row wake produces an entropy decrease which is not plausible and does not compare favorably with the measurements. This is due to the closure not mimicking the true unsteady wake chopping effect. The dominant effect of the downstream blade row is captured by including the front half of the airfoil. This effect is the metal blockage of the downstream airfoil and the bending of the wake streamlines due to the turning of the downstream blade row. The blockage effect of the upstream wake through the first half of the blade row is also still captured. Research is currently underway to correctly model the physics without truncating the grids, but the truncated grid approach can still provide a quality solution if the solution is interrogated correctly. The LPT rig simulation did not suffer from this problem so overlaps of one blade row were used. For the HPT rig and full turbine, a half blade row overlap was used for each blade row.

Model for Real Gas

A model for real gas effects which treats γ (the ratio of specific heats) as a linear function of temperature was presented by Turner (1996). In that implementation, γ was treated as an axisymmetric quantity. With the new closure implementation, this has been generalized so γ is now a three-dimensional quantity. This is very important for a turbine where the inlet total temperature can vary by 1000 degrees Rankine, and large variations in temperature can occur circumferentially due to wakes and secondary flows. Figure 3 shows how well the linear model compares with the actual real gas for γ, C_p (the specific heat at constant pressure) and H (the enthalpy) for a range of temperatures typical in an HPT at takeoff conditions. These quantities are also shown assuming a perfect gas at constant γ, resulting in a large enthalpy shift. With cooling flows modeled as sources of mass, momentum and energy, this allows the cooling flow to enter at the correct enthalpy level in order to achieve the correct energy balance.

One other assumption which has been used is that the ideal gas constant, R, is constant. For a cooled turbine in an engine environment, there are products of combustion in the flow entering the first stage turbine nozzle, However, the cooling flow does not have these products of combustion. This gas property difference leads to a

different R. The energy source term of the cooling flow described below accounts for this effect, although this leads to erroneous coolant film temperatures and other errors. A more correct approach is to track the products of combustion with a species equation and use a variable R. This has not yet been implemented so an average R for the turbine has been used.

Source Terms to Represent Cooling Flow

A source term approach described by Hunter (1998) is used to simulate the film cooling on the cooled airfoils, the endwalls and for some of the gaps with purge cavity flows. Sources of mass, momentum, energy and the turbulence quantities are specified in each cell adjacent to a surface with film injection. A row of cooling holes is actually modeled as a slot because the grid is not fine enough to capture the effect of each discrete film hole. Several inputs are required to specify the source terms. These include the coolant mass flow, the geometric angles of the hole centerline, the hole size, the coolant supply temperature, an approximate discharge static pressure, the turbulence intensity and the turbulent length scale of the coolant. With this information, the mass flux, energy flux, turbulent kinetic energy flux, turbulent dissipation flux and the total momentum flux can be determined. The source term in a cell is then set to the calculated flux. The unit vector of the momentum flux is specified tangent to the hole centerline, so the momentum flux in all three directions can be specified. This approach picks up the macroscopic effects of film cooling so the overall mass, momentum and energy are correct with the momentum applied at the correct angle relative to the blade or endwall surface. Figure 4 shows the contours of absolute total temperature on the pressure side of HPT nozzle 1 for the engine configuration. Clearly visible are the rows of cooling holes.

Leakage Model

In addition to the source term approach, there is a method to specify endwall leakage due to shroud leakage and purge flows. This method is applied as a code input. It differs from the source term approach in that the axial and radial momentum terms are updated as the solution converges. The leakage model is more straightforward to apply. Figure 5 shows how this model is applied to the under-shroud hub leakage across LPT nozzle 2. The velocity vectors crossing the endwall show where the leakage model has been applied. Also notice how the hub flowpath has been specified to model the real nozzle hub geometry. The effect of leakage is quite pronounced on the endwall temperature profiles. The amount, temperature and level of swirl for the leakage is input and held fixed as the solution converges. This input can be calculated from an assumed pressure drop across an orifice with a specified flow coefficient. This process has been automated using a proprietary labyrinth seal analysis code that requires the clearance, pressure drop and seal teeth arrangement as inputs. These leakage flows were then held fixed for the average passage analysis.

TURBINE SIMULATION CONFIGURATIONS

Figure 6 shows the geometry modeled in this study. For each of the configurations, total pressure, total temperature, the radial flow angle and zero swirl were specified at the inlet. At the exit, the static pressure was specified. For both rig configurations, the design intent geometry was used.

The goal of the rig measurements, the data reduction, and the choice of instrumentation used for these rigs has been to obtain turbine performance. The use of these data for validation of CFD simulations is only a byproduct of this primary goal. The biggest impact is that the energy output of a turbine is measured through a torque measurement of the shaft. Torque times wheel speed gives the power. The temperature measurements are taken to obtain radial variations in temperature and not the absolute level. The variation is obtained accurately without detailed calibration of the thermocouples. This detailed calibration is therefore not done. Static pressure measurements are taken under nozzle platform overlaps in the hub of a turbine. Due to detailed cavity aerodynamics, this is not the flowpath static pressure. In addition, upstream turbulence has not been measured. Upstream turbulence intensity values of 5% have been applied for the HPT and LPT rigs, and 10% for the full engine.

High Pressure Turbine Rig

The HPT rig geometry is shown in Figure 6. It is a ¾ scale cooled rig of the actual GE90 HPT which was designed and built at GE Aircraft Engines and has been tested at a NASA Glenn Research Center test cell. The actual configuration also included the strut and first LPT nozzle. Only the first four blade rows have been analyzed here. A simulation was set up to match the rig test conditions.

Low Pressure Turbine Rig

The LPT rig geometry, shown in Figure 6, is a ½ scale rig which was designed and built by GE and Fiat, and tested at GE. It is a six stage high efficiency LPT. As shown, the turbine center frame and turbine rear frame struts were tested and included in the analysis. This simulation was set up to match the rig test conditions at the LPT design point.

Full Engine Turbine Configuration

The full turbine configuration is shown in Figure 6 at full scale as it exists in the engine. A few changes relative to the rig designs had to be implemented for the production engine. The most notable is that the first stage nozzle throats had to be opened up to allow more flow in the growth production design. Overall boundary conditions and levels of cooling flow were set up using a cycle model of the GE90 at sea level takeoff, and at 0.25 Mach number. This cycle model has empiricism derived from rig and engine data and represents a good macroscopic view of the engine. The temperature profile at the inlet to the turbine is based on analysis and testing of the GE90 dual annular combustor at takeoff. Detailed distribution of cooling flow is based on analysis models of the serpentine passage cooling circuits. To match the cycle flow, the HPT nozzle throat area was increased 1.7% relative to design intent. This was accomplished by re-staggering the nozzle 0.35 degrees more open. This is a very small angle difference and was rationalized that area measurement error and assembly tolerance which is estimated at approximately 2% is greater than this change. Correct work splits among the stages and the future mating with the rest of the turbofan engine analysis requires that the mass flow be consistent with the cycle. This was accomplished by adjusting the throat area in a reasonable way.

RESULTS

Each simulation has been run until the axial variation in flowrate accounting for cooling and leakage flows became less than 0.2%.

Other parameters were also monitored to verify that the losses and work were not varying. Use of mass flow as an overall guide is appropriate for this subsonic turbine application. Because the multistage matching changes the mass flow, the mass flow for this application only settles out after other quantities have settled out. For each simulation, small changes in the simulation parameters have been made as the solution evolved. These included the nozzle re-stagger described above and a modification of coolant supply temperatures for the cooled turbine based on a re-evaluation of the assumptions. None of these cases were started from scratch and run to convergence without a simulation parameter change. The full turbine simulation took about 20,000 Runge-Kutta iterations with 50 iterations per flip or outer iteration. If the full turbine simulation was started from scratch with no changes in simulation parameters, it is expected that convergence could be achieved in about 10,000 iterations. The rig simulations take less time because of the reduced axial extent over which pressure and vortical waves need to travel.

Table I is a comparison of the rig analyses with experiment for one-dimensional overall quantities. The results compare well except that the flow is high in the HPT and low in the LPT relative to the experiment. It is not known why the HPT flow is high, but as mentioned above, a very small change in flow angle makes a big difference in flow. There can also be differences in actual throats relative to what was analyzed due to measurement and manufacturing tolerances. Coolant injection angles, especially at the trailing edge slots, also strongly affect the flowrate, but may not be modeled accurately. The LPT throats are not as difficult to measure as in the HPT since the exit angle is not as large. Therefore the geometry is probably not the cause of the discrepancy in the LPT. More likely, it may be due to the assumption in the turbulence model that the flow is fully turbulent, whereas in the rig there may be a large amount of laminar flow which would reduce the wakes and increase the flow. The temperature ratios do not match well, especially for the LPT. These values are also not consistent with the efficiency prediction which exhibits better agreement with the rig tests. As explained below, this is because the temperature measurements are made to obtain the profile shape, not the level, since the overall temperature levels are not rigorously calibrated in the experiments. A torque measurement is made to get the overall work from which efficiency is determined.

Table I. Comparison of Overall Performance of HPT and LPT Rig Analyses Relative to Experiment. Efficiency is analysis minus measured. Other quantities are (analysis - measured)/measured.

Case	Flow	Pressure Ratio	Temperature Ratio	Efficiency
HPT Rig (4 blade rows)	**+2.5%**	**+0.4%**	**-1.6%**	**-1.0%**
LPT Rig (14 blade rows)	**-2.5%**	**+0.3%**	**-3.5%**	**-0.5%**

Profiles of total pressure (PT), total temperature (TT) and angle are shown in Figures 7-9. Rig and engine analyses are compared with experimental data. At station 41, the PT and TT are normalized by the average PT and TT at station 4 (the inlet). At all other stations, PT and TT are normalized by the average plane 42 PT and TT values of the experiment or the cycle.

In Figure 7, the PT profiles at plane 42 show excellent agreement between the HPT rig analysis and data. The engine simulation profile is more hub-strong than the rig, while the LPT rig analysis profile is flat here since this plane represents the inlet of the LPT rig. At station 48, the strut loss and boundary layer in the LPT rig are well matched. At station 5, the shape and level match very well.

The TT profiles in Figure 8 at station 41 show the main difference between a rig and engine; namely the inlet combustor TT profile carries through nozzle 1 (although mixed) and has large gradients, especially near the hub relative to a flat inlet profile entering a rig. At station 42, relative to the experiment, the TT profile shows good agreement except near the hub where the experiment is slightly cooler than the prediction. The engine was instrumented with temperature rakes downstream of the HPT, and the full turbine simulation compares very well to these at station 48. At station 5, the full turbine comparison has the same overall gradient, but the midspan temperatures are calculated to be higher than the experiment. The LPT rig comparison of TT at station 5 shows good agreement. The overall difference is reflected in the 3.5% temperature ratio difference shown in Table I, which could be due to measurement calibration error.

The angle profiles are shown in Figure 9. At station 41, the full engine HPT nozzle 1 has been opened up to allow more flow and higher thrust since the rig was built. This is why the flow angle between full turbine and HPT rig are different. The swirl differences are not great between rig and full turbine at station 42. At station 48, the swirl at the LPT nozzle 1 leading edge in the full turbine simulation is different than design intent in the outer 20% span by as much as 10 degrees. At station 5, the LPT rig and measurement match well, and full turbine and LPT rig show little difference.

Figures 10 and 11 show the HPT and LPT rig static pressure comparison between analysis and experiment. The overall pressure drops are very large, so this same information has also been tabulated in Table II and Table III for the HPT rig and LPT rig respectively. The pressure taps in the rig are recessed in small gaps in the casing and mounted under the nozzle platform overlaps in the hub. This is why the location is described relative to the upstream or downstream nozzle platform in the tables. In general, the comparisons are very good. The hub pressures compare less well than the casing pressures which is likely due to the location of the pressure taps within the cavities. These cavities are not modeled in the analysis. The inlet total pressure profile and the exit static pressure profile are specified

which sets the overall total to static pressure ratio of the turbine. The inter-stage static pressure is therefore a result of the work splits among the stages and the reaction of each stage, which is a product of the turbine simulation. The good pressure comparison demonstrates that both work splits among the stages and reaction are correctly simulated.

Table II. Comparison of HPT Rig Hub and Casing Static Pressure. Quantities represent (analysis - measured)/(HPT rig overall total pressure drop).

HPT Rig Location	Casing	Hub
Stage 1 HPN Downstream Platform	**0.63%**	**1.86%**
Stage 2 HPN Upstream Platform	**No Data**	**-1.30%**
Stage 2 HPN Downstream Platform	**0.30%**	**0.87%**
Strut Forward Platform	**-1.34%**	**-0.91%**
Strut LE Rake Plane	**0.60%**	**0.12%**

Table III. Comparison of LPT Rig Hub and Casing Static Pressure. Quantities represent (analysis - measured)/(LPT rig overall total pressure drop).

LPT Rig Location	Case	Hub
Nozzle 1 Downstream Platform	**-0.04%**	**0.41%**
Nozzle 2 Upstream Platform	**-1.42%**	**0.76%**
Nozzle 3 Downstream Platform	**No Data**	**-2.43%**
Nozzle 4 Downstream Platform	**0.47%**	**-0.18%**
Nozzle 5 Upstream Platform	**-0.50%**	**0.37%**
Nozzle 5 Downstream Platform	**-0.60%**	**No Data**
Nozzle 6 Upstream Platform	**-1.39%**	**No Data**
Nozzle 6 Downstream Platform	**-0.31%**	**-1.43%**
Outlet GV Upstream Platform	**-0.24%**	**-0.22%**

These three configurations represent the three-dimensional flowfields of 36 blade rows. These are complex flowfields with variable properties, cooling flows and large secondary flows. There are many interesting features. One of these is visualized in Figure 12, which shows streamlines that were launched in the purge flow just upstream of LPT rotor 1. In the engine configuration, the amount of purge flow entering here is quite large relative to the rig. The streamlines get caught up in the hub vortex and lift off the hub surface. Downstream of the rotor is a contour plot of total temperature showing that the cold fluid emanated from the purge cavity.

Multistage Effects

Many axisymmetric solvers used in quasi-3D turbomachinery design systems use a blockage factor or flow coefficient as a sole parameter to account for many effects not described by the axisymmetric equations. One of these effects is due to circumferential variations within the flowfield. This approach of using blockage has a basis in matching measurements given total pressure, total temperature, angles, static pressure and overall flow rate. The only way to match the flow rate is by introducing a blockage factor which is less than one. For a given definition of average quantities, such as mass averaged enthalpy, area averaged static pressure, enthalpy averaged total pressure, mass averaged angular momentum and a momentum averaged meridional angle, one can determine this blockage factor from post processing any 3D solution. Because of the definition, this blockage is due to any circumferential variations including wakes, tip clearance flows, secondary flows, leakage flows and potential effects.

The blockage calculated in this way for the full turbine configuration is shown in Figure 13. The circumferential variations are especially large in the HPT where the temperature varies by over one thousand degrees Rankine due to cooling flow wakes and the secondary flows which act on the large inlet radial temperature gradients. In addition, the total pressure and static pressure vary tremendously. Values of this blockage factor less than 0.8 exist over large regions of the HPT. This means over 20% of the flow area is "blocked" in these regions due to these circumferential variations. These effects must be adequately modeled or the static pressure comparisons shown in Figures 10 and 11 and Tables II and III would not be so good. In addition to work splits and reaction, the thrust balance of the engine can be better simulated. Adamczyk (1999) has described flow blockage as being related to the recovery energy thickness and then related this to the unsteady deterministic flow state. This unsteady deterministic flow state is modeled well using the average passage approach and allows these effects to be captured. This is not the case for a mixing plane approach where the circumferential variations are eliminated across the mixing plane.

Other flow features become apparent in Figure 13 and this type of plot can demonstrate some overall characteristics of the simulation with one axisymmetric plot. Some of these features are the tip clearance flows downstream of the HPT rotors. The hub leakage effects can also be seen in the HPT and LPT.

Another multistage effect is that the static pressure downstream of a nozzle is very different with and without the rotor behind it. This is due to the blade blockage and turning of the downstream rotor and the high exit angle of the nozzle. Figure 14a shows the static pressure field predicted from an isolated blade row solver. The average exit radial static pressure profile has been imposed which comes from a streamline curvature axisymmetric solver. The boundary condition of this code holds this imposed average static pressure while allowing variations in the circumferential direction. Due to the high exit angle of the nozzle, the circumferential variations persist far downstream. Figure 14b shows the corresponding plot from an average passage solution. Notice how the isobars are altered by the close proximity of the rotor. The circumferential variations are attenuated by the rotor modeled as body forces. These apply the correct turning, energy drop and blade blockage to simulate the rotor downstream of the nozzle.

PARALLEL COMPUTING CAPABILITY

As mentioned above in the description of the solver, the code has two levels of parallel capability as shown in Figure 1. Achieving good parallel performance with this code requires that it be load balanced. Figure 15 shows how this has been done with the full turbine 18 blade row simulation. The size, geometry and aerodynamics of each blade row is different, and therefore the grid size varied. The load balancing was accomplished by assigning a blade row a fraction of processors equal to the fraction of grid relative to the total number of grid points. As shown in Figure 15, this leads to an imperfect load balancing because the number of processors is integral. The load balance improved slightly by increasing the number of processors from 60 to 121.

Figure 16 shows the parallel efficiency for APNASA run on an SGI ORIGIN 2000. The parallel performance of an isolated blade row calculation up to 8 processors is shown and demonstrates excellent parallel efficiency. With 2 processors, the speed-up is actually super linear, possibly due to reduced cache memory misses. The real test of the parallel performance is with the real full turbine simulation. The speedup is plotted against the number of processors assigned to blade row 2. A case with an equal number of processors per blade row is also shown and demonstrates the importance of optimal load balancing. Also shown are the 60 and 121 processor calculations which used 4 and 8 processors on blade row 2, respectively. The resulting parallel efficiency is 87.3% using 121 processors which truly demonstrates the case is well load balanced and the code has excellent parallel capability.

Currently the code takes 7.3×10^{-5} sec/grid-point/iteration on the 250 MHz SGI ORIGIN 2000 running in parallel with 121 processors. Since a solution starting from scratch would take approximately 10,000 iterations, a solution of the full turbine which has a total of nine million grid points would take 1820 processor hours. However, due to the parallel capability, this solution would be done in 15 hours of wall clock time utilizing 121 processors. This could be accomplished overnight, the key criteria for a code to be useful in the design environment.

The scenario for design use is that a design case can be run overnight. Automatic post-processing scripts could then be run at the end of the component simulation. The designer can then evaluate the design in the morning, make modifications, re-grid the new geometry and submit a new job to be run overnight. This process would continue until an optimal design is produced.

SUMMARY

Three GE90 turbine configurations have been analyzed using the average passage approach. Two of these are rig configurations where detailed data exists. The third is a full turbine configuration for the GE90 at a takeoff configuration. This simulation is the first dual-spool cooled turbine analyzed with a 3D multistage solver. Comparisons have been made to the measurements, and good agreement has been demonstrated. Multistage and component interaction effects have also been presented which demonstrate why a calculation such as this is worthwhile. The parallel efficiency of the code is excellent and can lead to effective use of this code in the design environment.

REFERENCES

Adamczyk, J.J., Mulac, R.A., and Celestina, M.L., 1986, "A Model for Closing the Inviscid Form of the Average-Passage Equation System," Journal of Turbomachinery, Vol. 108, pp. 180-186.

Adamczyk, J.J., 1999, "Aerodynamic Analysis of Multistage Turbomachinery Flows in Support of Aerodynamic Design," To be published at the 1999 ASME IGTI Conference.

Chen, J.P., Celestina, M.L. and Adamczyk, J.J., 1994, "A New Procedure for Simulating Unsteady Flows Through Turbomachinery Blade Passages," ASME Paper 94-GT-151.

Dawes, W.N., 1990, "Towards Improved Throughflow Capability: The Use of 3D Viscous Flow Solvers in a Multistage Environment," ASME Paper 90-GT-18.

Fritsch, G. and Giles, M.B., 1993, "An Asymptotic Analysis of Mixing Loss," ASME Paper 93-GT-345.

Hunter, S.D., 1998, "Source Term Modeling of Endwall Cavity Flow Effects on Gaspath Aerodynamics in an Axial Flow Turbine", Ph.D. Thesis, University of Cincinnati, Department of Aerospace Engineering and Engineering Mechanics, November.

Jameson, A. and Baker, T.J., 1984, "Multigrid Solutions of the Euler Equations for Aircraft Configurations," AIAA Paper 84-0093.

Kirtley, K.R., Turner, M.G. and Saeidi, S., 1999, "An Average Passage Closure Model for General Meshes," To be published at the 1999 ASME IGTI Conference.

Shabbir, A., Celestina, M.L., Adamczyk, J.J., and Strazisar, A.J., 1997, "The Effect of Hub Leakage Flow on Two High Speed Axial Flow Compressor Rotors," ASME Paper 97-GT-346, June.

Turner, M.G., 1996, "Multistage Turbine Simulations with Vortex-Blade Interaction," Journal of Turbomachinery, Vol. 118. pp. 643-653.

Turner, M.G., and Jennions, I.K., 1993, "An Investigation of Turbulence Modelling in Transonic Fans Including a Novel Implementation of an Implicit k-e Turbulence Model," ASME J. of Turbomachinery, Vol. 115. No. 2, April 1993, pp. 249-260.

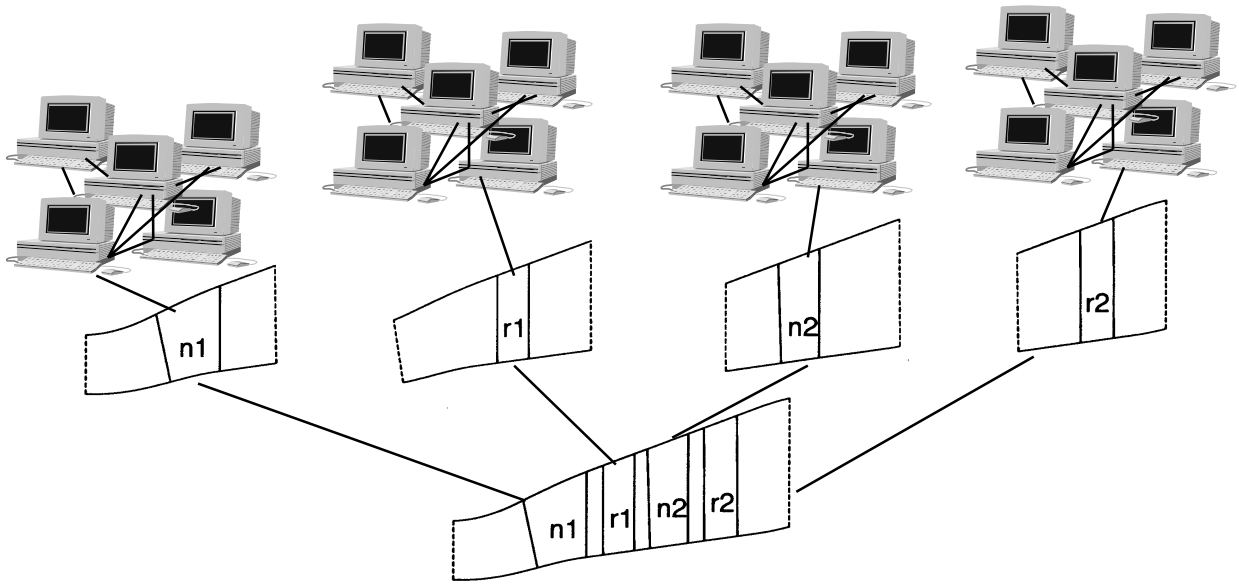

Figure 1. Two levels of parallel capability in Average Passage Code.

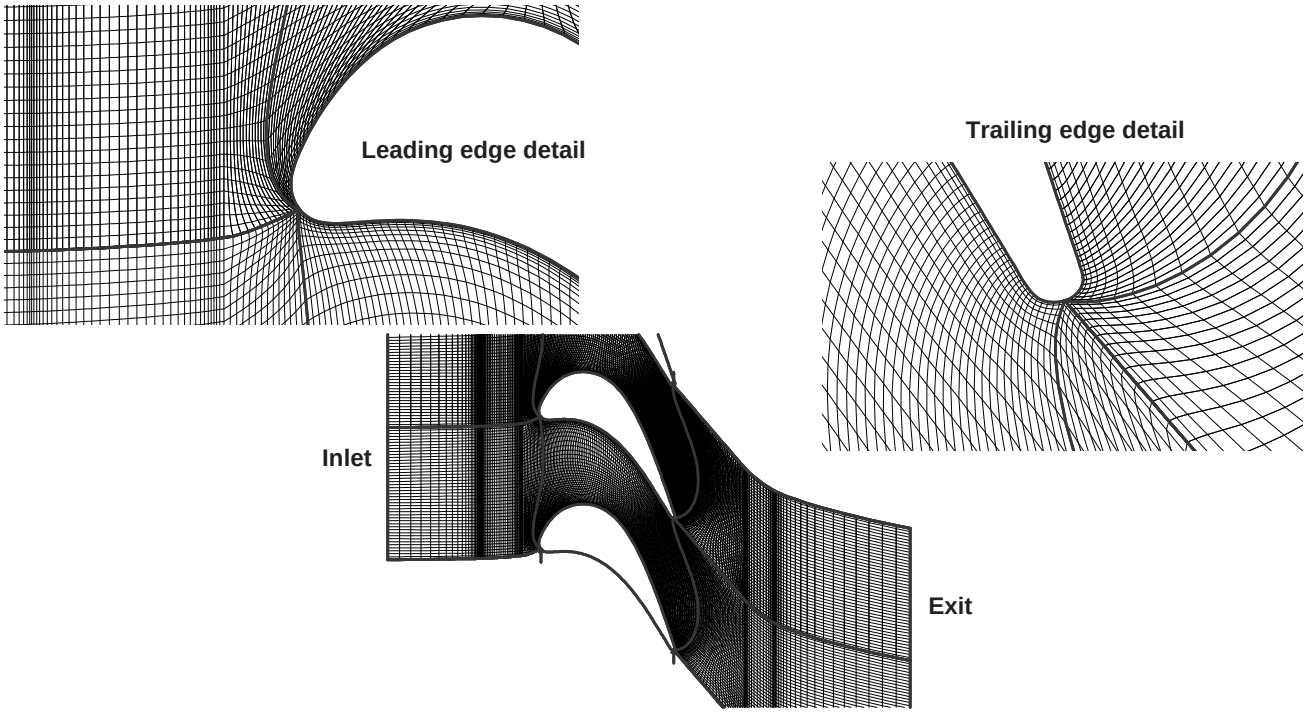

Figure 2. Blade-to-blade grid for the GE90 HPT rotor 1.

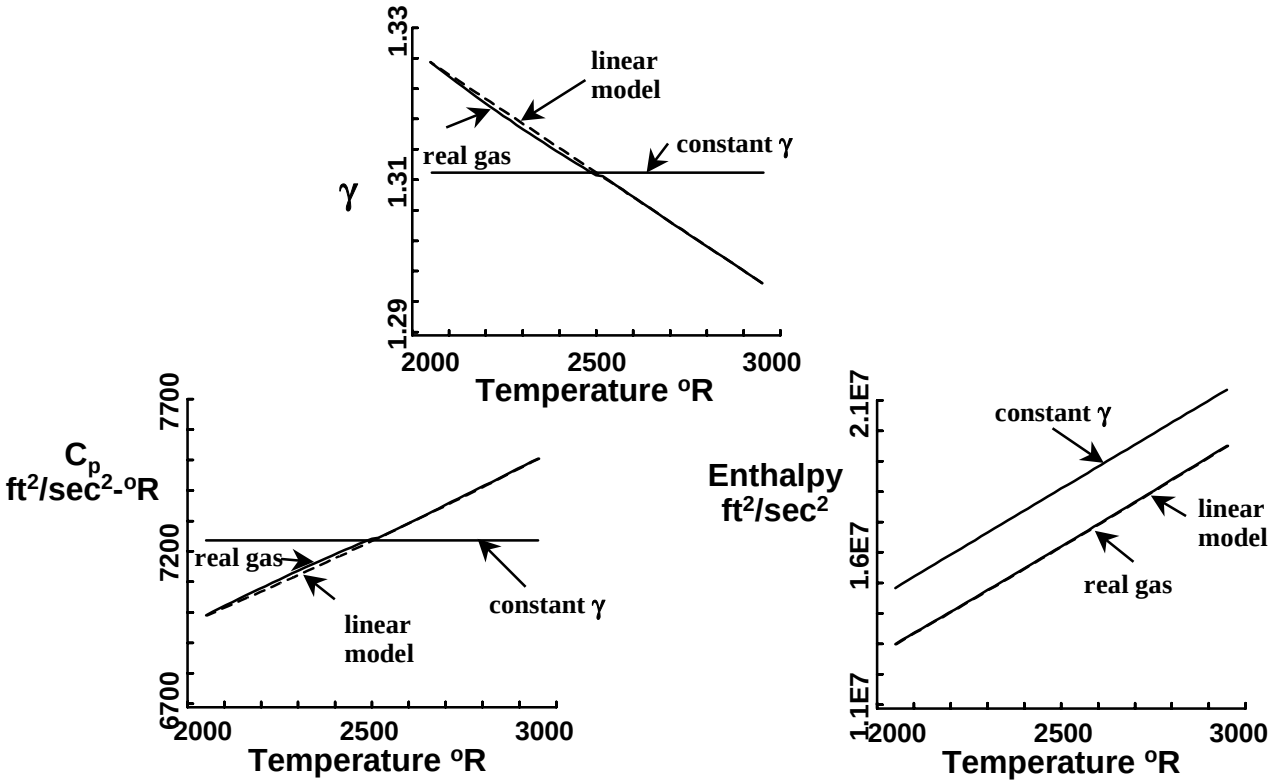

Figure 3. Linear real gas model used in Average Passage Code at HPT temperatures.

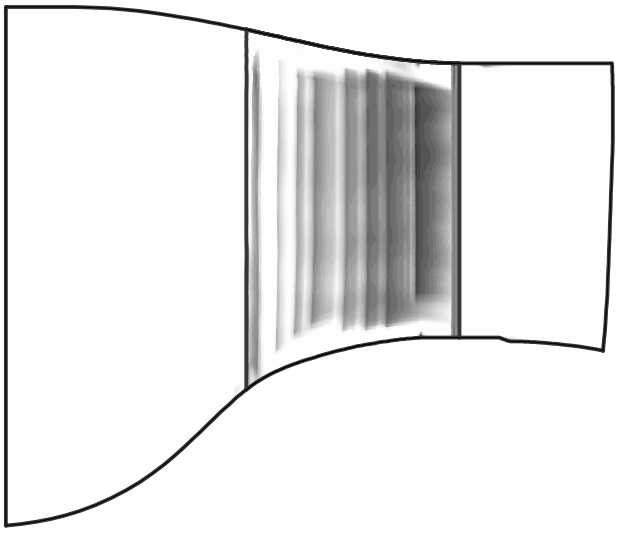

Figure 4. Total temperature contours of pressure side surface of nozzle 1 showing effect of the rows of film cooling holes. Dark - cold, light - hot.

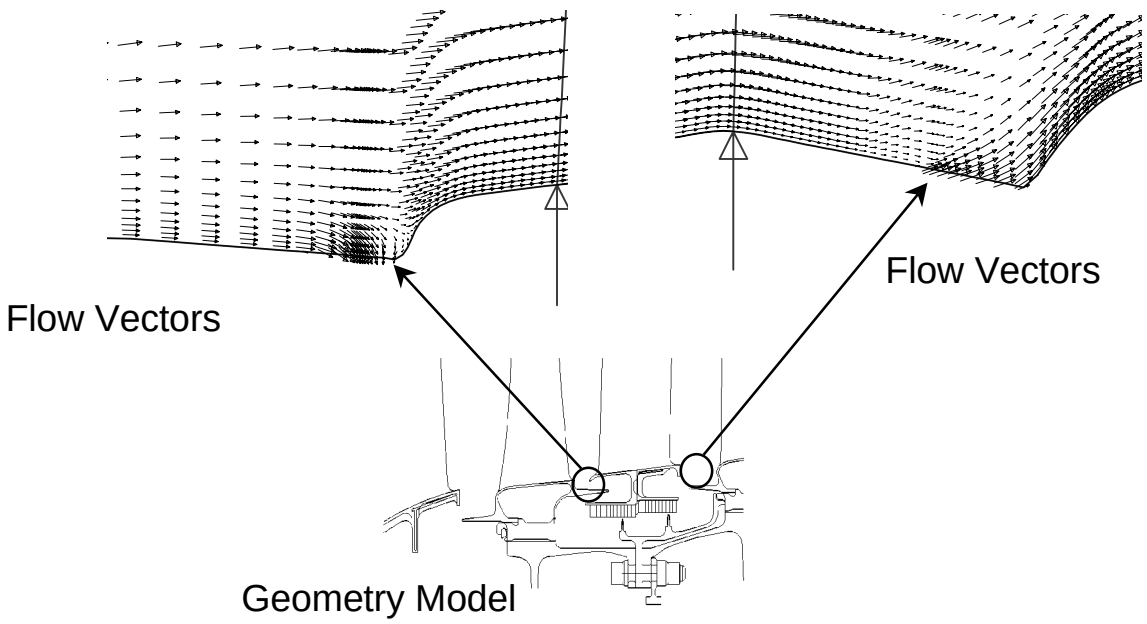

Figure 5. Application of leakage model.

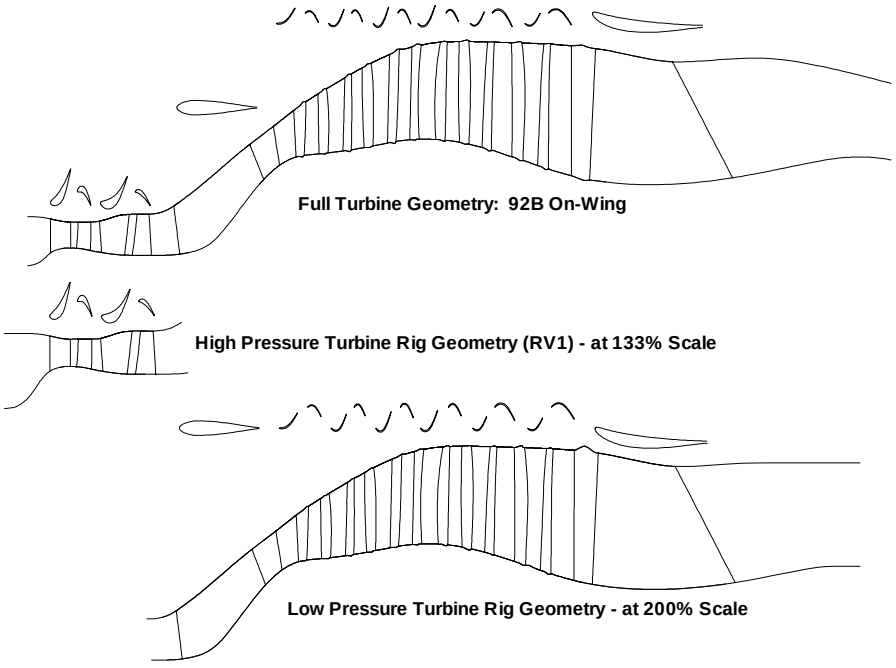

Figure 6. Geometry for full turbine, HPT rig and LPT rig.

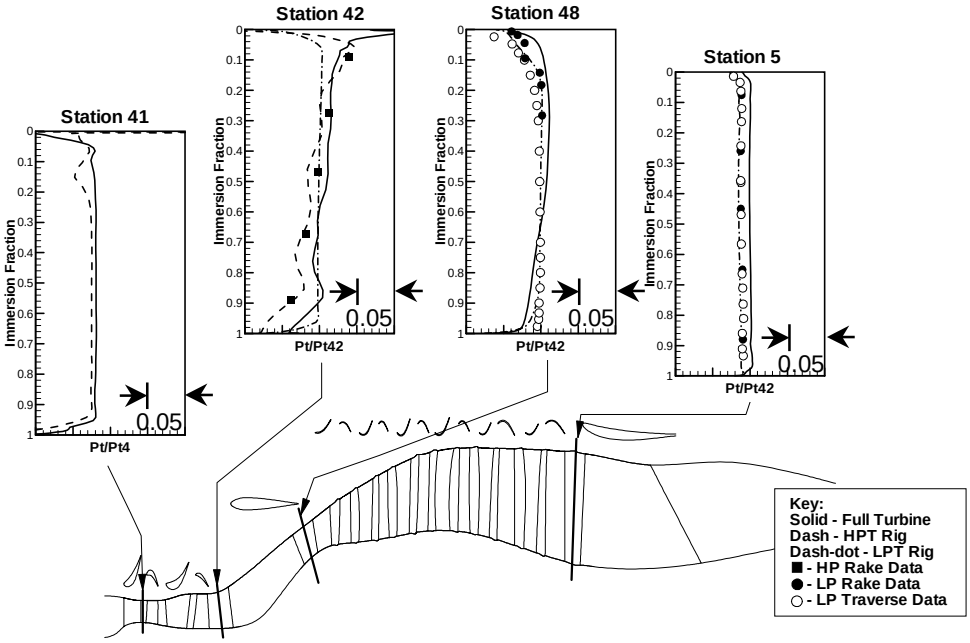

Figure 7. Total pressure profiles in turbine. Each major division is 5%.

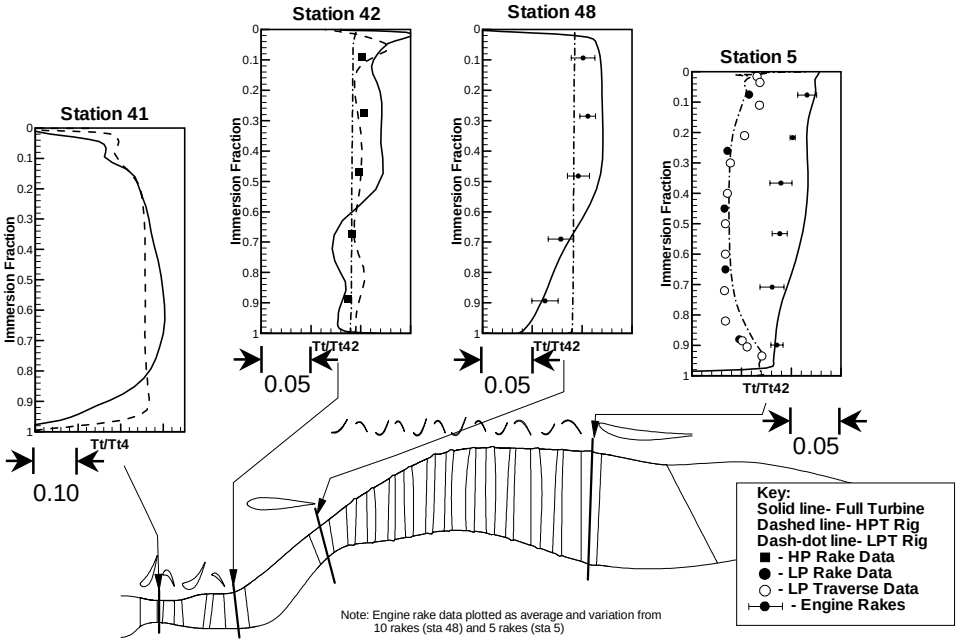

Figure 8. Total temperature profiles in turbine. The major division at station 41 is 10%. The major division for stations 42, 48 and 5 is 5%.

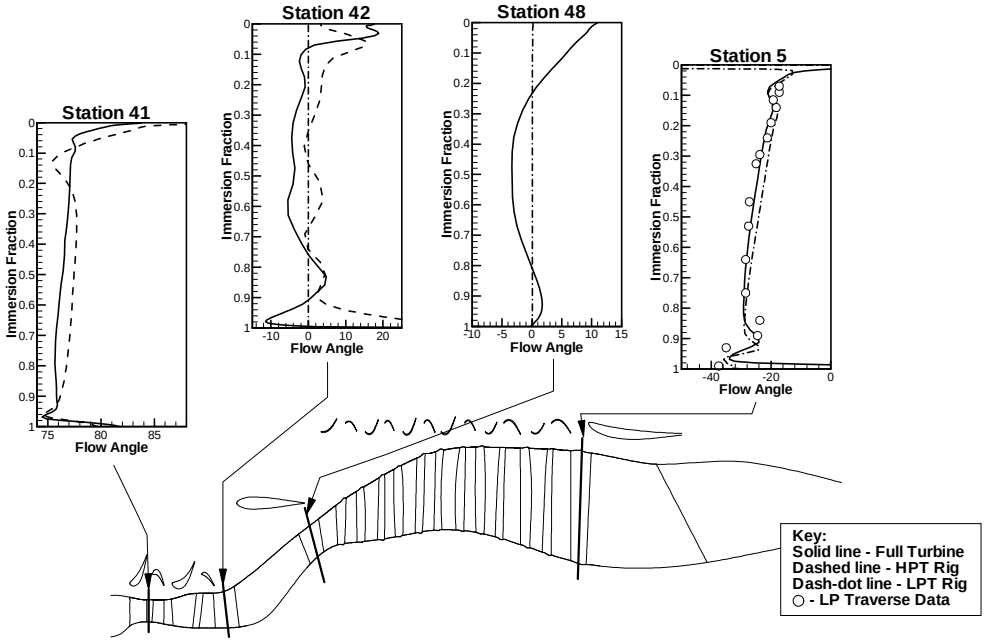

Figure 9. Absolute flow angle profiles in turbine.

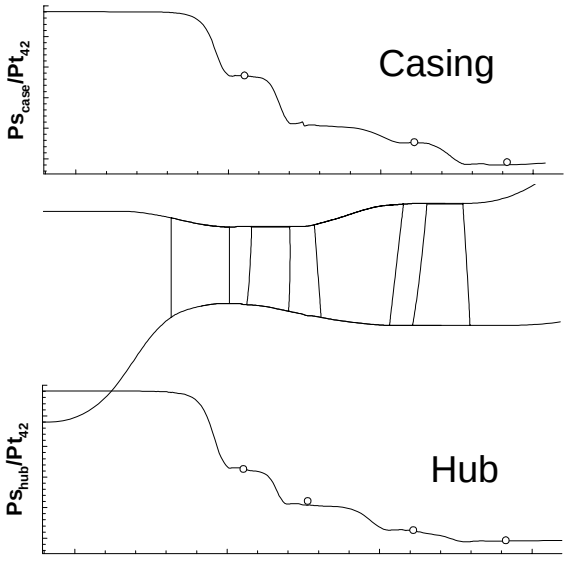

Figure 10. HPT Rig static pressure. Line - analysis, circle - data.

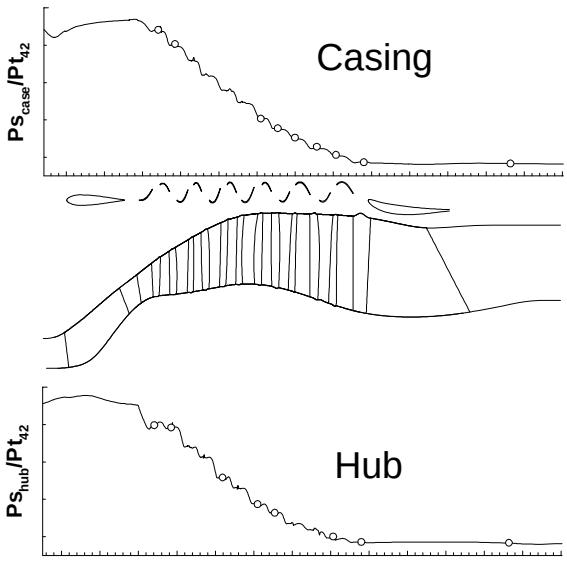

Figure 11. LPT Rig static pressure. Line - analysis, circle - data.

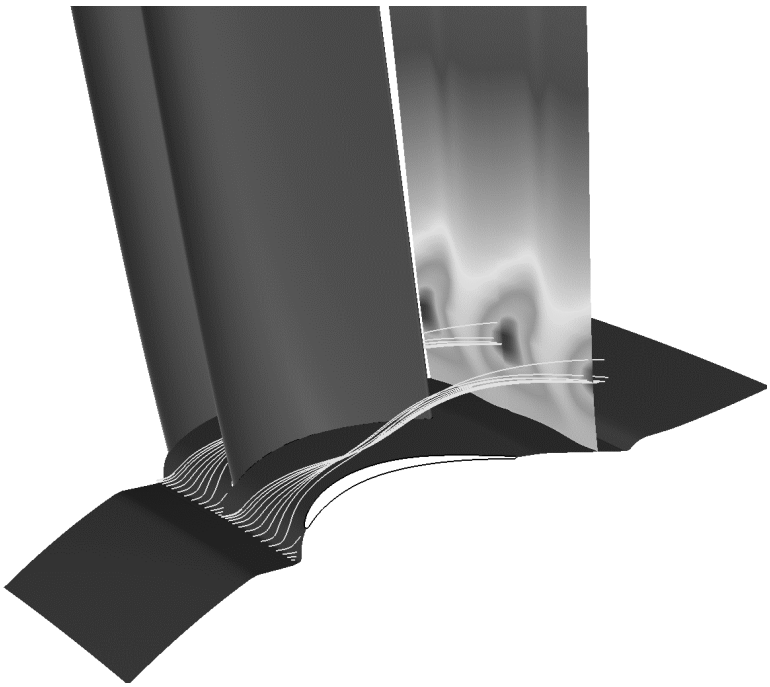

Figure 12. Streamlines showing purge flow caught in hub vortex. Plane downstream of trailing edge shows total temperature contours (dark-cold, light-hot). Full turbine simulation, LPT rotor 1.

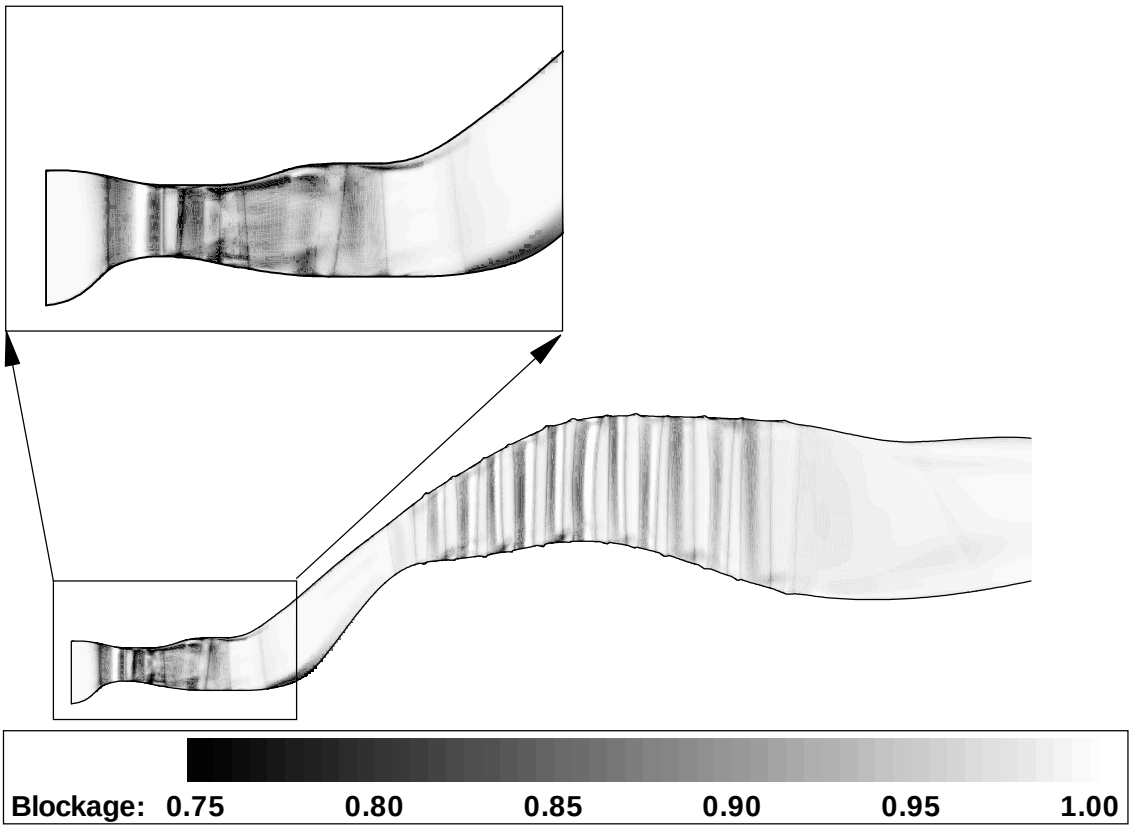

Figure 13. Contours of axisymmetric blockage for the full turbine configuration.

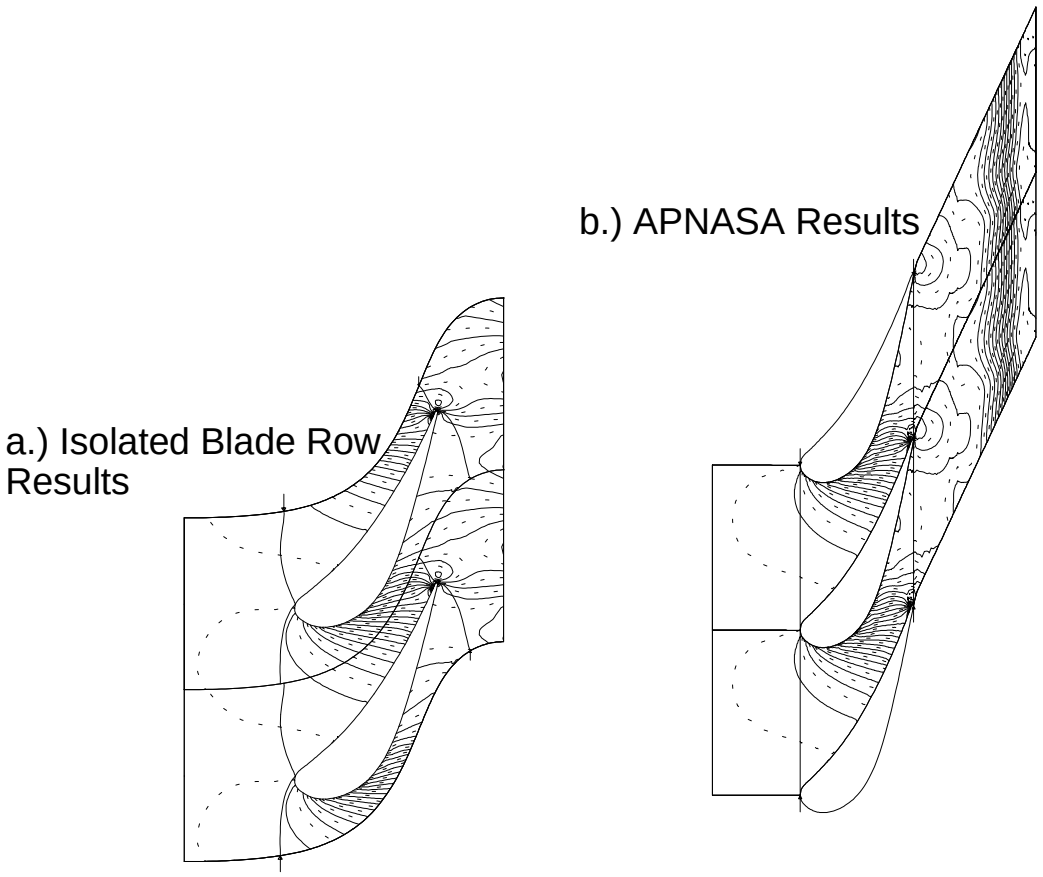

Figure 14. Static pressure contours for GE90 HPT nozzle 1 showing multistage effects.

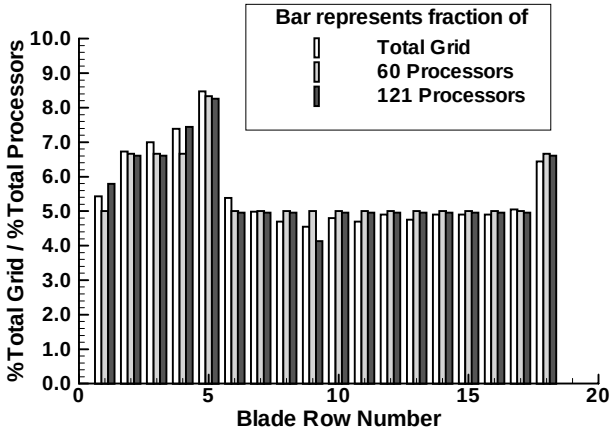

Figure 15. Load balancing based on grid size.

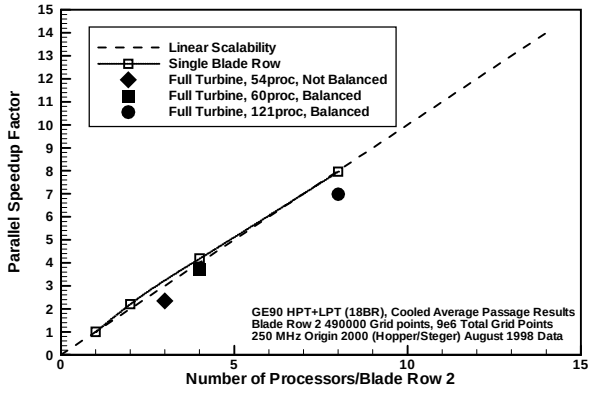

Figure 16. Parallel efficiency.

REPORT DOCUMENTATION PAGE

Form Approved
OMB No. 0704-0188

1. AGENCY USE ONLY (*Leave blank*)	2. REPORT DATE	3. REPORT TYPE AND DATES COVERED
	September 1999	Final Contractor Report

4. TITLE AND SUBTITLE

Multistage Simulations of the GE90 Turbine

5. FUNDING NUMBERS

WU–509–10–11–00
NAS3–26617

6. AUTHOR(S)

Mark G. Turner, Paul H. Vitt, David A. Topp, Sohrab Saeidi, Scott D. Hunter, Lyle D. Dailey, and Timothy A. Beach

7. PERFORMING ORGANIZATION NAME(S) AND ADDRESS(ES)

GE Aircraft Engines
One Neumann Way
Cincinnati, Ohio 45215

8. PERFORMING ORGANIZATION REPORT NUMBER

E–11880

9. SPONSORING/MONITORING AGENCY NAME(S) AND ADDRESS(ES)

National Aeronautics and Space Administration
John H. Glenn Research Center at Lewis Field
Cleveland, Ohio 44135–3191

10. SPONSORING/MONITORING AGENCY REPORT NUMBER

NASA CR—1999-209311

11. SUPPLEMENTARY NOTES

Prepared for the 1999 International Gas Turbine and Aeroengine Congress cosponsored by the American Society of Mechanical Engineers and the International Gas Turbine Institute, Indianapolis, Indiana, June 7–10, 1999. Paul H. Vitt, ASE Technologies, Cincinnati, Ohio; Mark G. Turner, David A. Topp, Sohrab Saeidi, Scott D. Hunter, and Lyle D. Dailey, GE Aircraft Engines, Cincinnati, Ohio; and Timothy A. Beach, Dynacs Engineering Company, Inc., Brook Park, Ohio. Project Manager, Joseph P. Veres, Computing and Interdisciplinary Systems Office, NASA Glenn Research Center, organization code 2900, (216) 433–2436.

12a. DISTRIBUTION/AVAILABILITY STATEMENT

Unclassified - Unlimited
Subject Categories: 07 and 64 Distribution: Nonstandard

This publication is available from the NASA Center for AeroSpace Information, (301) 621–0390.

12b. DISTRIBUTION CODE

13. ABSTRACT ***(Maximum 200 words)***

The average passage approach has been used to analyze three multistage configurations of the GE90 turbine. These are a high pressure turbine rig, a low pressure turbine rig and a full turbine configuration comprising 18 blade rows of the GE90 engine at takeoff conditions. Cooling flows in the high pressure turbine have been simulated using source terms. This is the first time a dual-spool cooled turbine has been analyzed in 3D using a multistage approach. There is good agreement between the simulations and experimental results. Multistage and component interaction effects are also presented. The parallel efficiency of the code is excellent at 87.3% using 121 processors on an SGI Origin for the 18 blade row configuration. The accuracy and efficiency of the calculation now allow it to be effectively used in a design environment so that multistage effects can be accounted for in turbine design.

14. SUBJECT TERMS

Gas turbines; Modeling; Flow; Simulation

15. NUMBER OF PAGES

19

16. PRICE CODE

A03

17. SECURITY CLASSIFICATION OF REPORT	18. SECURITY CLASSIFICATION OF THIS PAGE	19. SECURITY CLASSIFICATION OF ABSTRACT	20. LIMITATION OF ABSTRACT
Unclassified	Unclassified	Unclassified	